Next-to-Leading-Order QCD Corrections to $W^+W^-b\bar{b}$ Production at Hadron Colliders

A. Denner,[1] S. Dittmaier,[2] S. Kallweit,[3] and S. Pozzorini[4]

[1]*Institut für Theoretische Physik und Astrophysik, Universität Würzburg, 97074 Würzburg, Germany*
[2]*Physikalisches Institut, Albert-Ludwigs-Universität Freiburg, 79104 Freiburg, Germany*
[3]*Paul Scherrer Institut, Würenlingen und Villigen, 5232 Villigen PSI, Switzerland*
[4]*Institut für Theoretische Physik, Universität Zürich, 8057 Zürich, Switzerland*

(Received 18 December 2010; published 4 February 2011)

Top-antitop quark pairs belong to the most abundantly produced and precisely measurable heavy-particle signatures at hadron colliders and allow for crucial tests of the standard model and new physics searches. Here we report on the calculation of the next-to-leading order (NLO) QCD corrections to hadronic $W^+W^-b\bar{b}$ production, which provides a complete NLO description of the production of top-antitop pairs and their subsequent decay into W bosons and bottom quarks, including interferences, off-shell effects, and nonresonant backgrounds. Numerical predictions for the Tevatron and the LHC are presented.

DOI: 10.1103/PhysRevLett.106.052001 PACS numbers: 12.38.Bx, 12.38.Cy, 13.85.−t, 14.65.Ha

The top quark is the heaviest of all known elementary particles and is expected to play a key role in any theory of the flavor sector of elementary particles. Its precise investigation is, thus, of great importance at the current hadron colliders Tevatron and LHC, where top quarks are mostly produced via top-antitop ($t\bar{t}$) pairs.

The first step towards precise theoretical predictions for $t\bar{t}$ production at hadron colliders was made already about 20 years ago with the calculation of QCD corrections at next-to-leading order (NLO) [1–4]. Later also electroweak radiative corrections were calculated [5–8], and recently important progress has been achieved both in the resummation of logarithmically enhanced terms [9–12] and towards the inclusion of QCD corrections at next-to-next-to-leading order [13–23].

The above-mentioned predictions are based on the approximation of stable (on-shell) top quarks; i.e., the top-quark decays, which proceed into pairs of W bosons and b quarks in the standard model, were ignored. Recently, also studies [24–26] at the NLO QCD level have been presented that include the top-quark decays via a spin-correlated narrow-width approximation; i.e., the top quarks are still on shell. In this Letter we present first results (similar results on $WWbb$ production have recently been shown by the HELAC-OPP Collaboration [27]) at NLO QCD on the further generalization that the intermediate top quarks can be off their mass shell; i.e., we consider the process of $W^+W^-b\bar{b}$ production, including leptonic W-boson decays.

The reaction $pp \to W^+W^-b\bar{b} + X$ represents one of the few remaining $2 \to 4$ LHC background processes on the Les Houches wishlist [28]. While various such $2 \to 4$ NLO QCD calculations have been performed in recent years (see, e.g., Ref. [28] for a review), $W^+W^-b\bar{b}$ production involves the treatment of resonant particles for the first time in a hadron collider environment on that level of complexity. The two resonances can be consistently treated in the complex-mass scheme that was introduced at the NLO level in the context of the calculation of the electroweak corrections to the processes $e^+e^- \to WW \to 4$ fermions [29,30], which was the first full NLO calculation for a $2 \to 4$ particle process.

At leading order (LO), hadronic $W^+W^-b\bar{b}$ production proceeds via partonic channels with quark-antiquark ($q\bar{q}$) and gluon-gluon (gg) initial states. A few representative diagrams are depicted in Fig. 1. In addition to doubly resonant diagrams, where the $W^+W^-b\bar{b}$ final state results from the decay of a $t\bar{t}$ pair, our calculation also includes singly resonant and nonresonant contributions. As is well known, the bulk of the inclusive $W^+W^-b\bar{b}$ cross section is efficiently reproduced by the widely used narrow-width approximation, which incorporates all doubly resonant effects in the limit of vanishing top-quark width, $\Gamma_t \to 0$. By including all off-shell effects from doubly, singly, and nonresonant diagrams, our calculation consistently describes all contributions that are suppressed by one or more powers of Γ_t/m_t. These extra terms are mandatory in order to achieve percent-level precision in the (inclusive and differential) description of $t\bar{t}$ production, and for a reliable simulation of off-shell $W^+W^-b\bar{b}$ final states.

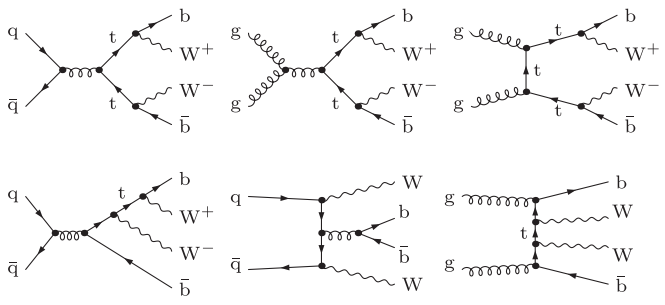

FIG. 1. Representative LO diagrams of doubly resonant (upper line), singly resonant (first diagram in lower line), and nonresonant type (last two diagrams in lower line).

To describe top-quark decays in a realistic way we also include the leptonic W-boson decays $W^+ \to \nu_e e^+$ and $W^- \to \bar{\nu}_\mu \mu^-$ in a spin-correlated narrow-width approximation.

In the following we briefly sketch the calculation of the virtual and real corrections. A more detailed description will be presented elsewhere. In order to prove the correctness of our results, we have evaluated each ingredient twice and independently. The treatment of the virtual QCD corrections to $q\bar{q}/gg \to W^+W^-b\bar{b}$ is based on diagrammatic representations of the one-loop amplitudes and numerical reduction of tensor integrals [31,32]. The $q\bar{q}$ and gg channels comprise about 300 and 800 one-loop diagrams, respectively. The most complicated ones are the 84 pentagons and 21 hexagons that contribute to the gg channel (see examples in Fig. 2) and involve tensor integrals up to rank five. Feynman diagrams are generated with two independent versions of FEYNARTS [33,34], and one-loop amplitudes are reduced along the lines of Refs. [35,36] using two in-house MATHEMATICA programs, one of which relies on FORMCALC [37] for preliminary manipulations. The employed approach strongly mitigates the complexity inherent in Feynman diagrams by exploiting factorization of color matrices, reduction of helicity structures to compact spinor chains, and recycling of a multitude of common subexpressions. The treatment of rational terms of ultraviolet or infrared origin is described in Appendix A of Ref. [35]. The reduced expressions are automatically converted into FORTRAN77 programs that evaluate color and helicity summed quantities with very high CPU efficiency. Tensor integrals are related to scalar integrals by means of numerical algorithms that avoid instabilities from inverse Gram determinants and other spurious singularities [31,32].

The presence of intermediate unstable top quarks in $pp \to W^+W^-b\bar{b} + X$ represents a nontrivial new aspect as compared to previous NLO QCD studies of multiparticle processes. To regularize intermediate top-quark resonances in a gauge-invariant way, we employ the complex-mass scheme [30]. In this approach the top-quark width Γ_t is incorporated into the definition of the renormalized (squared) top-quark mass, $\mu_t^2 = m_t^2 - im_t\Gamma_t$. In the on-shell scheme this complex parameter μ_t^2 is identified with the position of the pole of the top-quark propagator, and the top mass counterterm $\delta\mu_t$ is related to the top-quark self-energy at $p_t^2 = \mu_t^2$ via [see (4.25) in Ref. [30]]

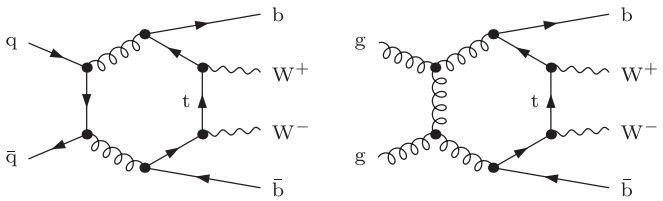

FIG. 2. Hexagon diagrams in $q\bar{q}/gg \to W^+W^-b\bar{b}$.

$$\delta\mu_t = \frac{\mu_t}{2}[\Sigma^{t,R}(\mu_t^2) + \Sigma^{t,L}(\mu_t^2) + 2\Sigma^{t,S}(\mu_t^2)]. \quad (1)$$

We note that an expansion of the occurring self-energies around the real point $p_t^2 = m_t^2$ [as, e.g., suggested in (4.27) in Ref. [30]] is not sufficient for NLO accuracy, because the top-quark self-energy is not analytic at the complex pole, $p_t^2 = \mu_t^2$. The evaluation of one-loop scalar box integrals in the presence of complex masses represents another nontrivial aspect of the complex-mass scheme. In our calculation we employ the results of Ref. [38], where explicit analytic continuations have been presented for all kinematic box configurations that are relevant for physical processes.

The real corrections receive contributions from the $2 \to 5$ partonic processes $gg \to W^+W^-b\bar{b}g$ and $q\bar{q} \to W^+W^-b\bar{b}g$, as well as from crossing-related gq and $g\bar{q}$ channels. The $2 \to 5$ matrix elements are evaluated with MADGRAPH [39] and, alternatively, using the Weyl–van der Waerden formalism of Ref. [40]. To isolate infrared divergences and cancel them analytically, we employ in-house implementations of the dipole subtraction formalism [41]. Specifically this is done in dimensional regularization with strictly massless light quarks (including b quarks) and alternatively in a hybrid scheme with small quark masses with the respective dipole subtraction terms from Ref. [42].

Color and helicity correlations that enter the subtraction procedure are generated by means of AUTODIPOLE [43] and, alternatively, in analytic form. To achieve sufficient numerical stability we perform the 11-dimensional phase-space integration using multichannel Monte Carlo techniques with weight optimization [44]. The integration of the dipole-subtracted $2 \to 5$ contributions is optimized by means of additional channels corresponding to the dipole kinematics.

In the following we present predictions for the Tevatron ($p\bar{p}$ collisions at 1.96 TeV) and the LHC (pp collisions at 7 TeV). In NLO (LO) QCD we employ MSTW2008NLO (LO) parton distributions [45] and describe the running of the strong coupling constant α_S with two-loop (one-loop) accuracy, including five active flavors. Contributions induced by the strongly suppressed bottom-quark density are neglected. For the gauge-boson and top-quark masses we use $m_t = 172$ GeV, $M_W = 80.399$ GeV, and $M_Z = 91.1876$ GeV. The masses of all other quarks, including b quarks, are neglected. In view of the negligibly small Higgs-mass dependence we adopt the $M_H \to \infty$ limit; i.e., we omit diagrams involving Higgs bosons. The electroweak couplings are derived from the Fermi constant $G_\mu = 1.166\,37 \times 10^{-5}$ GeV^{-2} in the G_μ scheme, where the sine of the mixing angle and the electromagnetic coupling read $s_w^2 = 1 - M_W^2/M_Z^2$ and $\alpha = \sqrt{2}G_\mu M_W^2 s_w^2/\pi$. For consistency, we perform the LO and NLO calculations using the top-quark widths $\Gamma_{t,\mathrm{LO}} = 1.4655$ GeV and $\Gamma_{t,\mathrm{NLO}} = 1.3376$ GeV [46], respectively. Since the leptonic W-boson decay does not receive NLO QCD corrections, we employ the NLO W-boson width $\Gamma_W = 2.0997$ GeV

everywhere. Final-state quarks and gluons with pseudorapidity $|\eta| < 5$ are converted into infrared-safe jets using the anti-k_T algorithm [47]. For the Tevatron (LHC) we set the jet-algorithm parameter $R = 0.4$ (0.5) and apply the transverse-momentum and pseudorapidity cuts $p_{T,b\text{-jet}} > 20$ (30) GeV, $|\eta_{b\text{-jet}}| < 2.5$. Moreover, we require a missing transverse momentum of $p_{T,\text{miss}} > 25$ (20) GeV and charged leptons with $p_{T,l} > 20$ GeV and $|\eta_l| < 2.5$.

The LO and NLO $W^+W^-b\bar{b}$ cross sections at the Tevatron and at the LHC are plotted in Fig. 3 as a function of the renormalization and factorization scales, $\mu_{\text{ren}} = \mu_{\text{fact}} = \mu$. At the Tevatron, where the cross section is dominated by the $q\bar{q}$ channel, at $\mu = m_t$ we obtain $\sigma^{\text{Tev}}_{\text{LO}} = 44.31^{+19.68}_{-12.49}$ fb and $\sigma^{\text{Tev}}_{\text{NLO}} = 41.75^{+0.00}_{-3.79}$ fb, where the uncertainties describe missing higher-order corrections estimated via scale variations in the range $m_t/2 < \mu < 2m_t$.

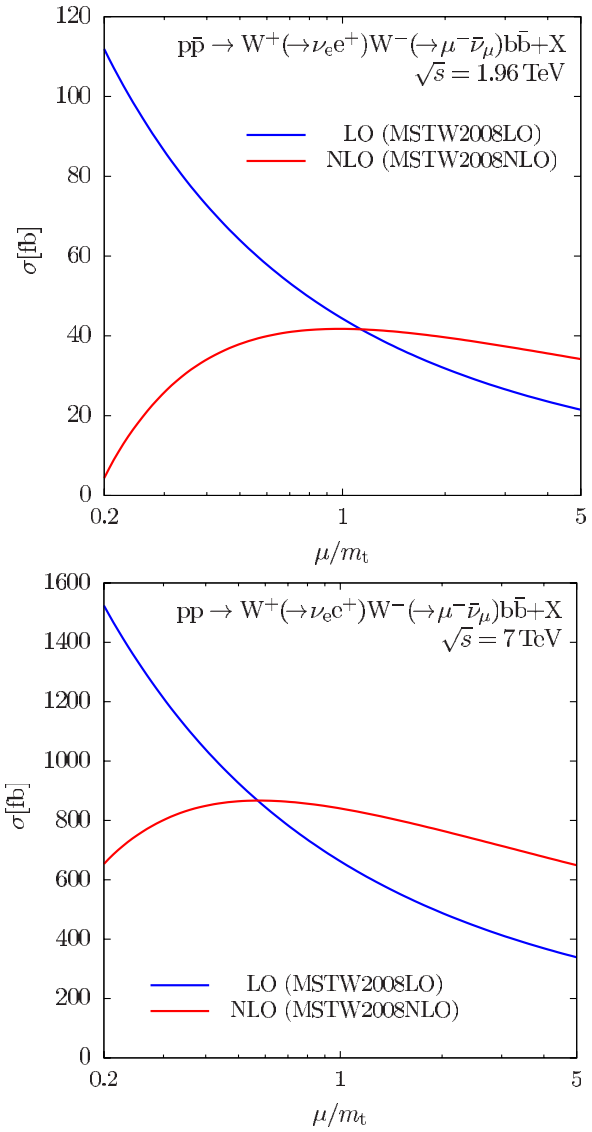

FIG. 3 (color online). Scale dependence of the LO and NLO $W^+W^-b\bar{b}$ cross sections at the Tevatron and the LHC.

For the LHC, where the gg channel dominates, we obtain $\sigma^{\text{LHC}}_{\text{LO}} = 662.4^{+263.4}_{-174.1}$ fb and $\sigma^{\text{LHC}}_{\text{NLO}} = 840^{+27}_{-75}$ fb. Normalizing the results to LO predictions at $\mu = m_t$ we obtain the relative NLO corrections $K^{\text{Tev}} = 0.942^{+0.000}_{-0.085}$ and $K^{\text{LHC}} = 1.27^{+0.04}_{-0.11}$. The NLO corrections induce a moderate shift of the integrated cross section and reduce its scale uncertainty from about 44% (40%) to 9% (9%) at the Tevatron (LHC). This confirms the good convergence of perturbative predictions at the scale $\mu = m_t$, a feature that is reflected also in the stable shape of the NLO curves in Fig. 3.

To assess the impact of finite-width effects on the integrated cross section we have extrapolated our numerical

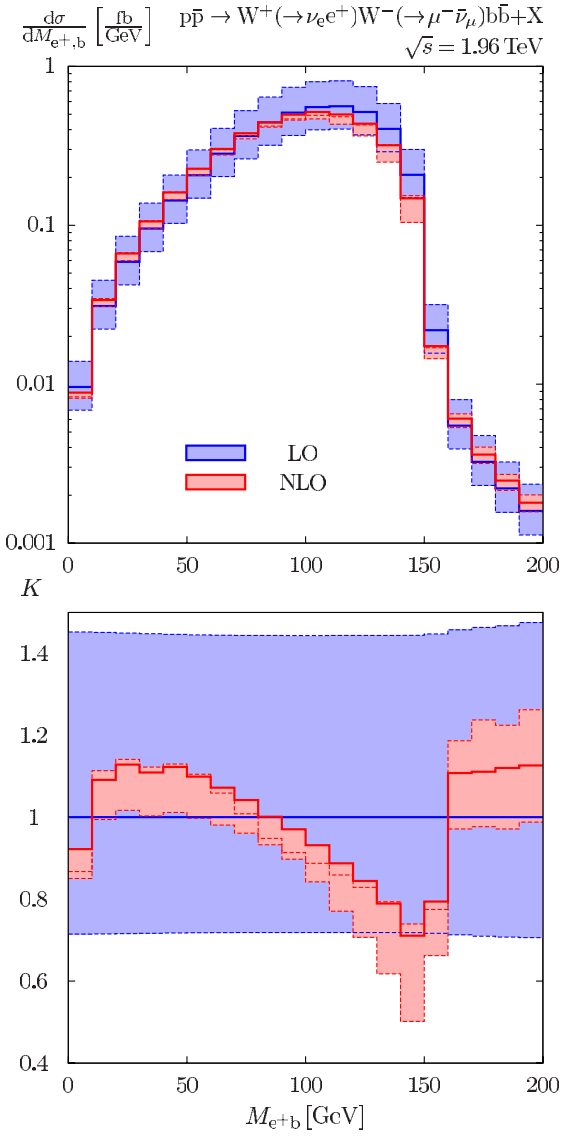

FIG. 4 (color online). Invariant mass M_{e+b} of the positron–b-jet system at the Tevatron: absolute LO and NLO predictions (upper plot) and relative corrections with respect to LO at $\mu = m_t$ (lower plot). The uncertainty bands describe $m_t/2 < \mu < 2m_t$ variations.

results to the narrow-width limit $\Gamma_t \to 0$. In this region we observe a linear Γ_t dependence, consistent with the cancellation of logarithmic soft-gluon singularities. At the Tevatron we find that finite-width effects shift the LO(NLO) cross section by about $-0.8\%(-0.9\%)$. At the LHC we observe a qualitatively different behavior: the shift induced by finite-width contributions is smaller in size and positive. At LO it amounts to $+0.4\%$, and at NLO it becomes as small as the Monte Carlo statistical error ($+ 0.2\%$).

To illustrate NLO and finite-width corrections to differential observables, in Fig. 4 we plot the invariant-mass distribution of a positron and a b jet—the visible products of a top-quark decay—at the Tevatron. In narrow-width and LO approximation this kinematic quantity is characterized by a sharp upper bound, $M^2_{e+b} \leq m_t^2 - M_W^2$, which renders it very sensitive to the top-quark mass. The value of m_t can be extracted with high precision using, for instance, the invariant-mass distribution of a positron and a J/ψ from a B-meson decay [48], an observable that is closely related to M_{e+b}. In Fig. 4 we clearly see, already in LO, small but non-negligible off-shell contributions that elude the kinematic bound. At NLO this feature becomes more pronounced, also due to QCD radiation that enters the b jet without being emitted from its parent b quark. Below the kinematic bound we find very significant NLO effects. In the region $50 < M_{e+b} < 150$ GeV the shape of M_{e+b} is strongly distorted, with corrections ranging from $+15\%$ to -30% (see lower plot). In the vicinity of the kinematic bound the NLO prediction is barely consistent with the LO uncertainty band. This example demonstrates the importance of $2 \to 4$ NLO predictions for a precise description of the kinematic details of the $W^+W^-b\bar{b}$ final state and, more generally, for the top-physics program at the Tevatron and at the LHC.

S. P. thanks the Swiss National Science Foundation for support. This work is supported in part by the European Community's Marie-Curie Research Training Network HEPTOOLS under Contract No. MRTN-CT-2006-035505.

Note added in proof.—Shortly after the submission of this Letter, results of a similar calculation by the HELAC-OPP Collaboration were published [49].

[1] P. Nason *et al.*, Nucl. Phys. **B327**, 49 (1989).
[2] W. Beenakker *et al.*, Nucl. Phys. **B351**, 507 (1991).
[3] M. L. Mangano, P. Nason, and G. Ridolfi, Nucl. Phys. **B373**, 295 (1992).
[4] S. Frixione *et al.*, Phys. Lett. B **351**, 555 (1995).
[5] W. Beenakker *et al.*, Nucl. Phys. **B411**, 343 (1994).
[6] S. Moretti, M. R. Nolten, and D. A. Ross, Phys. Lett. B **639**, 513 (2006).
[7] J. H. Kühn, A. Scharf, and P. Uwer, Eur. Phys. J. C **51**, 37 (2007).
[8] W. Bernreuther, M. Fücker, and Z.-G. Si, Phys. Rev. D **74**, 113005 (2006).
[9] M. Beneke, P. Falgari, and C. Schwinn, Nucl. Phys. **B828**, 69 (2010).
[10] M. Czakon, A. Mitov, and G. F. Sterman, Phys. Rev. D **80**, 074017 (2009).
[11] V. Ahrens *et al.*, J. High Energy Phys. 09 (2010) 097.
[12] N. Kidonakis, Phys. Rev. D **82**, 114030 (2010).
[13] S. Dittmaier, P. Uwer, and S. Weinzierl, Phys. Rev. Lett. **98**, 262002 (2007).
[14] B. Kniehl *et al.*, Phys. Rev. D **78**, 094013 (2008).
[15] C. Anastasiou and S. M. Aybat, Phys. Rev. D **78**, 114006 (2008).
[16] M. Czakon, A. Mitov, and S. Moch, Phys. Lett. B **651**, 147 (2007).
[17] M. Czakon, A. Mitov, and S. Moch, Nucl. Phys. **B798**, 210 (2008).
[18] M. Czakon, Phys. Lett. B **664**, 307 (2008).
[19] R. Bonciani *et al.*, J. High Energy Phys. 07 (2008) 129.
[20] R. Bonciani *et al.*, J. High Energy Phys. 08 (2009) 067.
[21] R. Bonciani *et al.* arXiv:1011.6661.
[22] A. Gehrmann-De Ridder and M. Ritzmann, J. High Energy Phys. 07 (2009) 041.
[23] M. Czakon, Phys. Lett. B **693**, 259 (2010).
[24] W. Bernreuther *et al.*, Nucl. Phys. **B690**, 81 (2004).
[25] K. Melnikov and M. Schulze, J. High Energy Phys. 08 (2009) 049.
[26] W. Bernreuther and Z.-G. Si, Nucl. Phys. **B837**, 90 (2010).
[27] G. Bevilacqua, http://indico.cern.ch/getFile.py/access?resId=22&materialId=slides&confId=91923.
[28] J. R. Andersen *et al.*, (SM and NLO Multileg Working Group), arXiv:1003.1241.
[29] A. Denner *et al.*, Phys. Lett. B **612**, 223 (2005).
[30] A. Denner *et al.*, Nucl. Phys. **B724**, 247 (2005).
[31] A. Denner and S. Dittmaier, Nucl. Phys. **B658**, 175 (2003).
[32] A. Denner and S. Dittmaier, Nucl. Phys. **B734**, 62 (2006).
[33] J. Küblbeck, M. Böhm, and A. Denner, Comput. Phys. Commun. **60**, 165 (1990).
[34] T. Hahn, Comput. Phys. Commun. **140**, 418 (2001).
[35] A. Bredenstein *et al.*, J. High Energy Phys. 08 (2008) 108.
[36] A. Bredenstein *et al.*, J. High Energy Phys. 03 (2010) 021.
[37] T. Hahn and M. Perez-Victoria, Comput. Phys. Commun. **118**, 153 (1999).
[38] A. Denner and S. Dittmaier, Nucl. Phys. **B844**, 199 (2011).
[39] J. Alwall *et al.*, J. High Energy Phys. 09 (2007) 028.
[40] S. Dittmaier, Phys. Rev. D **59**, 016007 (1998).
[41] S. Catani and M. H. Seymour, Nucl. Phys. **B485**, 291 (1997).
[42] S. Catani *et al.*, Nucl. Phys. **B627**, 189 (2002).
[43] K. Hasegawa, S. Moch, and P. Uwer, Comput. Phys. Commun. **181**, 1802 (2010).
[44] R. Kleiss and R. Pittau, Comput. Phys. Commun. **83**, 141 (1994).
[45] A. D. Martin *et al.*, Eur. Phys. J. C **63**, 189 (2009).
[46] M. Jezabek and J. H. Kühn, Nucl. Phys. **B314**, 1 (1989).
[47] M. Cacciari, G. P. Salam, and G. Soyez, J. High Energy Phys. 04 (2008) 063.
[48] A. Kharchilava, Phys. Lett. B **476**, 73 (2000).
[49] G. Bevilacqua *et al.*, arXiv:1012.4230.